



Validation and Verification  
for Aerospace Applications

# Assignment

Marc Barcelo  
December 2019

MSc Aerospace Computational Engineering

# Index

---

Abstract.....	5
Introduction.....	5
Theory Fundamentals .....	6
· Equations.....	6
· Turbulence Models.....	7
· Riemann Solvers.....	8
Characteristics of the Problem .....	9
Results .....	10
· Meshes performed.....	10
· Reference Model – Experimental Data.....	12
· Coarse Mesh:.....	14
· Medium Mesh:.....	16
· Fine Mesh:.....	18
Grid Convergence Study: Grid Convergence Index and Richardson Extrapolation.....	20
· Grid Convergence Index .....	20
· Richardson Extrapolation.....	24
Conclusions .....	25

Future work .....	27
Appendix 1: Grid Convergence Study .....	28
Appendix 2: Ground Effect Analysis .....	30
Appendix 3. Large Image of Fine Mesh: Experimental data, Riemann Solvers, and turbulence models. Upper Airfoil Surface, Detail of Figure 10 .....	34
References .....	35

## **List of Tables**

Table 1. Meshes, number of cells and boundary refinement relative to Coarse Mesh.....	11
Table 2. Grid Convergence Index.....	22
Table 3. Richardson Extrapolation.....	24

## **List of Figures**

Figure 1. Near boundary mesh representation of Tyrel 26 airfoil.....	9
Figure 2. Comparison between Experimental Data and RNG k- $\varepsilon$ model.....	13
Figure 3. Detail of Figure 1.....	13
Figure 4. Scaled Residuals for Coarse Mesh, RNG k- $\varepsilon$ turbulence model.....	14
Figure 5. Coarse Mesh: Pressure coefficient distribution for each turbulence model and Riemann Solver.....	15
Figure 6. Insight into Figure 5 .....	16
Figure 7. Scaled Residual for Medium Mesh, RNG k- $\varepsilon$ turbulence model .....	17

Figure 8. Medium Mesh: Pressure coefficient distribution for each turbulence model and Riemann Solver.....	17
Figure 9. Residuals for Fine Mesh and RNG $k - \varepsilon$ turbulence model, ROE-FDS solver. Converged solution at the 57 <sup>th</sup> iteration.....	18
Figure 10. Fine Mesh: Pressure coefficient distribution for each turbulence model and Riemann Solver.....	19
Figure 11. Comparison between Medium and Fine Mesh.....	20
Figure 12. Points selection for COARSE Mesh.....	21
Figure 13. Points selection for MEDIUM Mesh.....	21
Figure 14. Points selection for FINE Mesh.....	22

## **List of Equations**

(1) RANS Continuity .....	7
(2) RANS Momentum.....	7
(3) RANS Energy.....	7
(4) Richardson Extrapolation .....	24

## **Abstract**

The aim of this document is to evaluate the performance of a Tyrrell 26 airfoil in operation conditions by using different CFD available turbulence models -6 in total- in conjunction with two different Riemann solvers. The software used to run those simulations will be Ansys Fluent. Once obtained the results, a thorough comparison will be made in order to determine the advantages and cons of each case. Furthermore, the influence of the mesh quality will be also considered by analyzing coarse, medium and fine meshes of the same Tyrrell airfoil.

## **Introduction**

The importance of Computational Fluid Dynamics in our current society can be easily proven by looking into the research documents but also companies of a wide scope: from econometry to the original area: aerospace. The reason for its high applicability is the fact that Navier-Stokes equations are the most powerful tool humans have to describe any flow that surrounds us: from simple water to meteorological phenomena but even also to city complex flows of people and cars.

However, the nature of those equations – fully introduced in the 19<sup>th</sup> century- make them quite unsolvable by analytical means. Even a generous prize (1M \$) has been set by Clay Institute of Mathematics after defining it as one of the “Millennium Problem” to anybody who draws further information on this barely known but analytically hostile equations. That is why, CFD has consequently been largely developed as an acceptable solution to obtain the desired variables though numerical methods and as said, it is widely used in current industry but investigation as well.

Hence, for the problem faced: A Tyrrell 26 (Classic Formula 1 Car) airfoil facing flow with  $5^\circ$  of angle of attack and  $M=0.0874$ ; a study based on CFD software/methods and using Reynolds-Averaged Navier-Stokes equations will be conducted in the following lines.

However, we have been asked to use one of the 6 turbulence models applied as a reference, in my case, it is the RNG  $k - \varepsilon$  model. Since experimental data is available for the current airfoil in (Zerihan, 2001), it will be firstly compared to our reference turbulence model to graphically see the general accuracy achieved for each mesh.

## Theory Fundamentals

### • Equations.

The numerical methods and schemes will operate under the restrictions of the Navier-Stokes Equations. Since the problem is not time dependent, hence steady state, the local term of the equation will disappear. This, following Reynolds' Decomposition, will lead the problem to be solved under the Reynolds-Averaged Navier-Stokes equations (RANS). Another CFD approximations, such as U-RANS, LES, DNS and other hybrid methods, could be more accurate but would redound in further computational time.

As the objective of this module is to perform analysis of 36 CFD simulations in academic environment and to get in touch with elementary CFD software –FLUENT- this approximation will be valid for now. Serve the following equations visible in: (Jakirlić et al., 2007) as the three main equations (continuity, momentum, energy) for compressible flows to be solved for our CFD method:

$$\frac{\partial \bar{\rho}}{\partial t} + \frac{\partial}{\partial x_j} (\bar{\rho} \tilde{U}_j) = 0 \quad (1)$$

$$\frac{\partial(\bar{\rho} \tilde{U}_i)}{\partial t} + \frac{\partial}{\partial x_k} (\bar{\rho} \tilde{U}_i \tilde{U}_k + \bar{\rho} \widetilde{u''_i u''_k}) = - \frac{\partial \bar{P}}{\partial x_i} + \frac{\partial \bar{\tau}_{ik}}{\partial x_k} \quad (2)$$

$$\frac{\partial(\bar{\rho} \tilde{E})}{\partial t} + \frac{\partial}{\partial x_k} (\bar{\rho} \tilde{H} \tilde{U}_k + \bar{\rho} \widetilde{u''_i u''_k} \tilde{U}_i) = \frac{\partial}{\partial x_k} (\bar{\tau}_{ik} \tilde{U}_i) - \frac{\partial}{\partial x_k} (\bar{q}_k + \bar{q}_k^{(t)}) + \bar{\rho} D_{kk} \quad (3)$$

#### • Turbulence Models.

The evaluated turbulence models will be the following:

- Spalart-Allmaras
- Standard  $k-\varepsilon$ .
- **RNG  $k-\varepsilon$** .
- Realizable  $k-\varepsilon$ .
- Standard  $k-\omega$ .
- SST  $k-\omega$ .

Note that RNG  $k-\varepsilon$  is highlighted through bold characters. This is due to the fact that it will serve as reference for comparing the others with this one. Every turbulence model, as seen in the module “Modelling Approaches for Aerospace Applications”, has its own lights and shadows and main fields to be applied. Hence, it is not chosen because of its applications – the one that suits the problem better will be proven in the following lines- but because arbitrarily I have been asked to perform it.

Thus, let me introduce briefly the main characteristics of the RNG  $k-\varepsilon$  turbulence model.

According to the useful website CFD online ([https://www.cfd-online.com/Wiki/RNG\\_k-epsilon](https://www.cfd-online.com/Wiki/RNG_k-epsilon))

[epsilon model](#)), this method performs really alike to the standard k-epsilon model, with the exception that epsilon equation is treated differently. Although slight improvements have been noticed in terms of rotation treatments in contrast to the standard theory, it is not used as it was expected to. The main applicability of them is related with indoor air CFD modelling.

#### • **Riemann Solvers.**

The results of the turbulence models for each mesh will be computed serving two different Riemann Solvers. Consequently, it will provide us further knowledge to appreciate which may be more convenient to our case and to determine the overall performance of each.

The Riemann Solvers used will be the following:

- ROE-FDS (Roe Flux Differencing Scheme)
- AUSM (Advection Upstream Splitting Method)

On the one hand, the ROE-FDS solver is firstly developed by Phil Roe –then corrected by Harten- and based on the powerful Godunov scheme. The hostile non-linear terms are solved through special linear interpolations. The correction introduced by Harten mainly consisted of the application of smoothing techniques to make non-physical results from simple Roe method to physical, especially in  $M \sim 1$  where shockwaves appear.

On the other hand, AUSM –proposed by Liou and Steffen- bases its function on the upwind scheme to deal with inviscid flows. Its main methodology is the separation of the problem into advection (convection) and pressure fluxes, corresponding to linear and non-linear terms. It has been proven to deal successfully with a wide variety of problems: any kind of Mach number, LES, DNS, shock wave detections, aeroacoustics, etc.

Hence, they both seem perfect candidates to solve our RANS equations and their performance will be discussed in the conclusions section.

## Characteristics of the Problem

Allow me to refresh compact the characteristics of our problem in this section and which is going to be solved immediately.

The evaluated Airfoil belongs to a Tyrell 26 car which has been already modelled and meshed like in the following image:

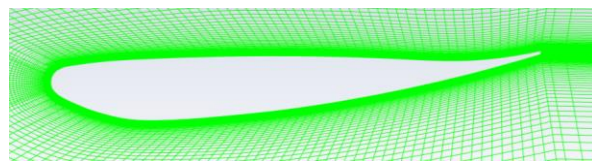


*Figure 1. Near boundary mesh representation of Tyrel 26 airfoil*

Additionally, the operation conditions are:

- Angle of Attack (AoA): 5 (Freestream)
- Pressure/Gauge Pressure: 101325 Pa
- Reynolds Number:  $4.6 \times 10^5$
- Temperature: 293 K
- Mach number: 0.0874

These conditions will be introduced in the Ansys-Fluent software for farfield and outflow conditions to serve as our boundary conditions. Since it is a steady problem, initial conditions are not needed. However, there's not an option to insert the Reynolds number but it gives us an idea that convective forces are dominant against viscosity. Then, flow can be considered as inviscid.

Also, Fluent does not have an option to introduce the AoA directly, but the unitary vectors of the flow can be specified. This is why, for x component, the unitary vector will be  $\cos(5) = 0.9961947$  and for y,  $\sin(5) = 0.0871557$ . Ideal density and Sutherland law for viscosity may be also inputted.

However, Mach number is really low ( $M=0.0874$ ) and therefore fluid can be truly considered to be incompressible ( $M < 0.3$ ), but according to the compulsory solvers (ROE-FDS and AUSM) to be applied, they want us to apply the compressible theory (density-based).

## Results

### • Meshes performed

The idea of applying 3 meshes –coarse, medium and fine- is to analyze the influence of the grid resolution in the accuracy of the solution. Nevertheless, it has not been specified the cells or configuration required for each mesh, then each has been configured by the author's criteria minding about computational time, solution accuracy and stability, and after a huge amount of failures and little successful results. The cells configured, then, converge for all turbulence models in acceptable computational time -around 7 minutes as worst case scenario- which is not a trivial condition at all.

The Courant Number –which theoretically should be  $<1$  to obtain converged physical solutions- has been set for all the cases to the value of 2 since in a practical view, it also drives to reliable results. Even CFD experiments have used Courant Values of 200 and relied of the results. However, we tried to achieve sharp results with no appreciable oscillations in the residuals and in the spectra of the  $c_p$ .

The number of cells for each mesh has been the following:

*Table 1. Meshes, number of cells and boundary refinement relative to Coarse Mesh*

Mesh	Cells	Refinement of boundary layer
Coarse	23976	-
Medium	45576	x 2
Fine	53610	x 100

For the Coarse Mesh, it is directly used the provided mesh without performing any further refinement/coarsening.

When refining, to achieve better results without increasing hugely the computational time or complexity, only the boundary-layer near field will be refined. This will lead from having a structured mesh to an unstructured one. However, results will not lose reliability.

To refine, a new boundary section of the radial 30 cells normal to the airfoil will be selected and refined. It does not mean that 30 cells will be only selected, but that the sum of all 30 cells in each normal direction from the foil.

For the Medium Mesh, the refinement factor has been 2 (relative to coarse mesh) and for the Fine Mesh, 100 (relative to coarse mesh too). However, cells do not seem to behave proportionally. Since not the whole mesh has been refined, it is not logic that refining the “normal 30 cells section” is approximately the double of the coarse mesh, and a factor of 100 only results

in “the triple”. However, the numbers introduced were those and I must rely on them. Nevertheless, there have been several issues when performing those meshes and running simulations that did not behave logically – meshes coarser with same data were increasing residuals until finally these results were obtained after several days of simulating.

Once explained the meshing performed, we will properly run the calculations to obtain the following results.

#### • Reference Model – Experimental Data.

A total of 36 (2 solvers \* 3 meshes \* 6 turbulence models) simulations have been run and hence a lot of data, figures and comparisons can be displayed in this document. However, the logical first step to carry out is to compare our turbulence reference model (RNG k– $\varepsilon$ ) with the experimental data ( $C_p - X/C$ ) for each mesh.

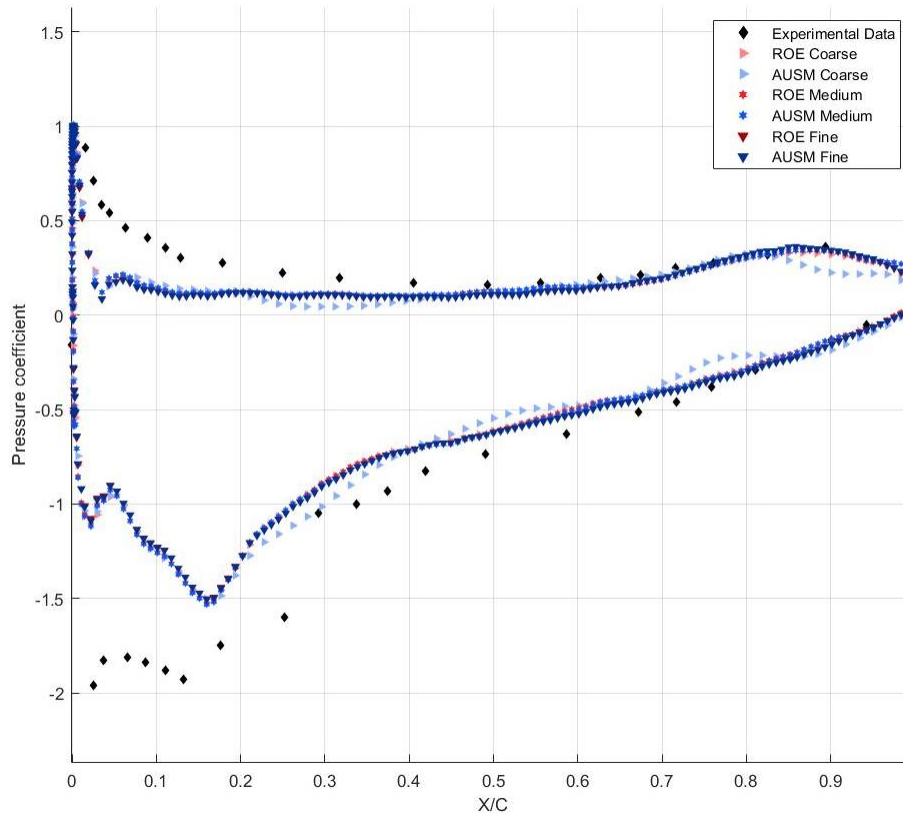


*Figure 2. Comparison between Experimental Data and RNG k- $\varepsilon$  model*

As it can be seen, the RNG k- $\varepsilon$  model remains quite accurate to the experimental data.

The Riemann solver used does not seem to have great influence on the result either. As meshes get refined, model points are available and less fluctuations can be seen – solution gets more stable. However, between “Fine” and “Medium” meshes there are not too much difference, actually most of them overlap. In order to appreciate more detail, a zoom will be made into the previous Figure 2.

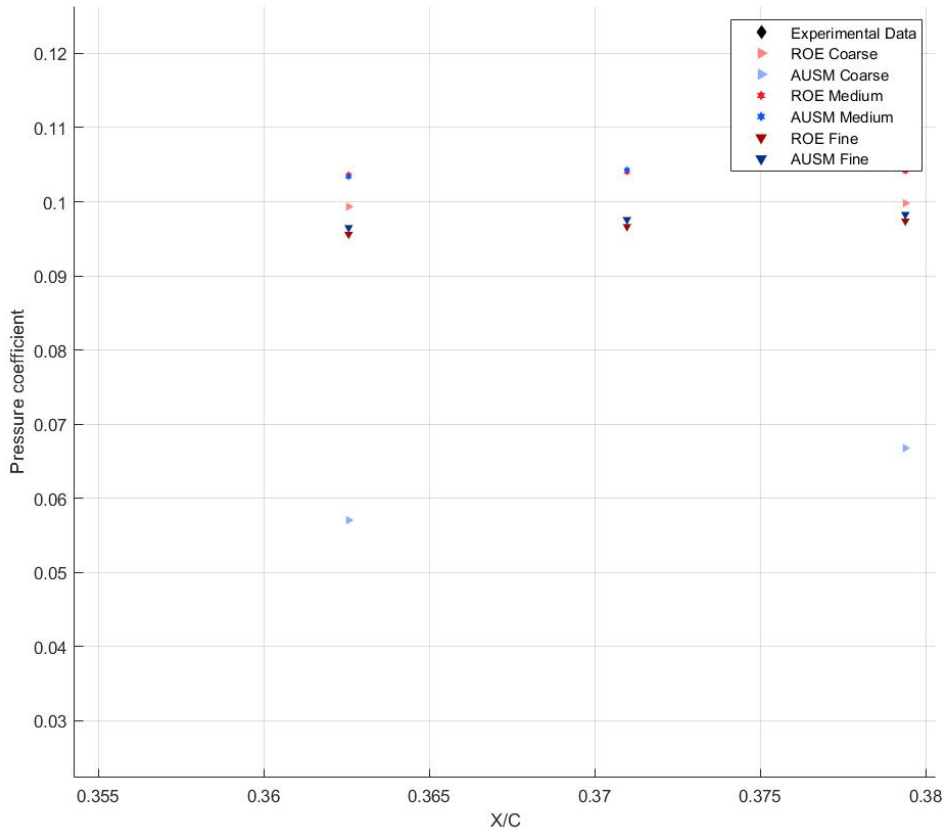


*Figure 3. Detail of Figure 1*

Now this Figure 3 does achieve to show points with so little coincidence of different solvers/meshes. If even more detail wants to be seen in order to further compare the turbulence models, please see Appendix 3. Large Image of Fine Mesh: Experimental data, Riemann Solvers,

and turbulence models. Upper Airfoil Surface, Detail of Figure 10 Only in the medium grid, for both AUSM and ROE-FDS solvers, there is a so tiny difference that one is overlapped with the other. Nevertheless, an important fact is revealed: for the Coarse Mesh, the ROE-FDS Riemann solver accomplishes better performance than the AUSM, whilst for others they have not barely difference at all. What is even more astounding is the fact that ROE-FDS for Coarse Mesh also run more alike the fine mesh than the medium.

Once it is seen that, overall, the accuracy of the reference RNG  $k-\varepsilon$  model to the Experimental Data is quite acceptable, we will see how the other turbulence models for the three meshes and two Riemann solvers behave relatively. From now on, the RNG  $k-\varepsilon$  numerical solutions will be plotted as scattered black dots in order to be distinguished more easily.

#### • Coarse Mesh:

Overall, according to (Figure 4), the iterations made for the Coarse Mesh in all the turbulence models has been 2500, yet the convergence of the solution has not been achieved at any case. As convergence solution criteria, the value of  $10^{-6}$  has been for all the components seen in the Figure 4 and extra that take part in other methods such as  $k$ ,  $\varepsilon$  and  $\omega$ .

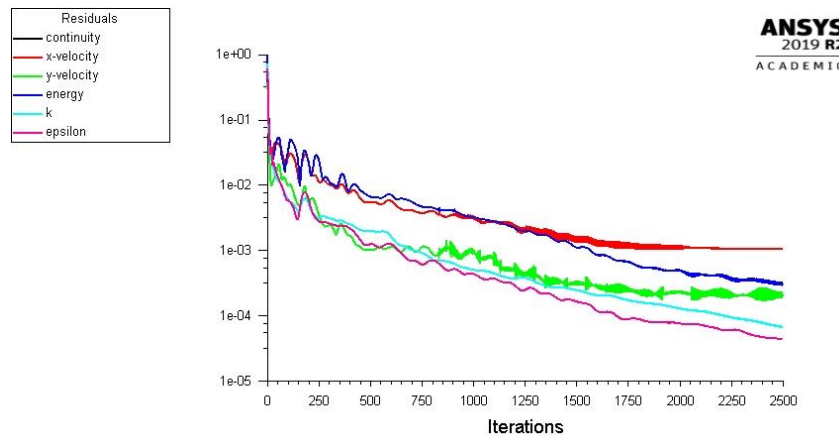
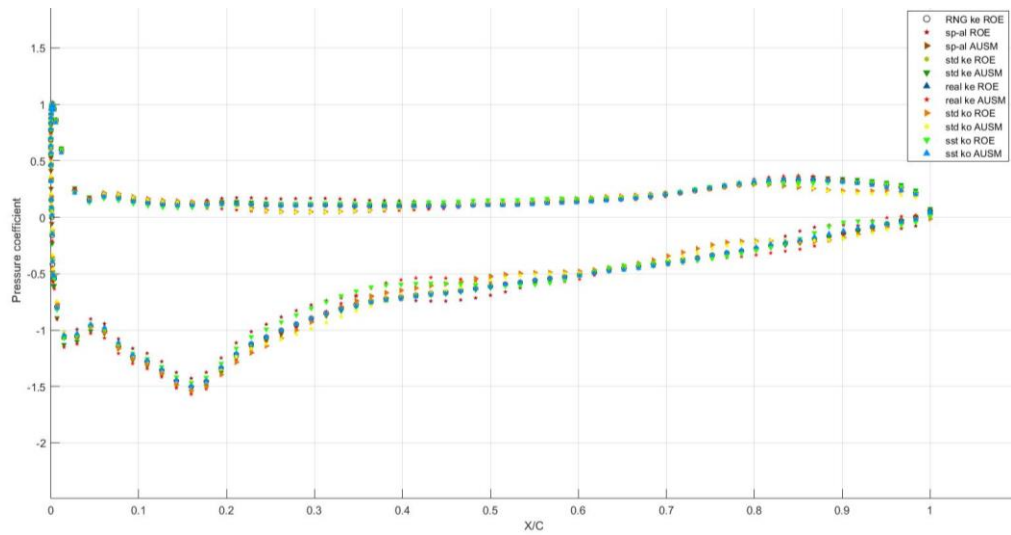


Figure 4. Scaled Residuals for Coarse Mesh, RNG  $k-\varepsilon$  turbulence model

However, as it can be seen, they remain considerably low and getting lower at a slow rate so it can be assumed that solution will reliable, even it took 4:54.88 minutes to perform 2500 iterations.

Since it is the mesh where more deviation in results can be expected, we will present the 6 turbulence models for each Riemann solver in Figure 5.



*Figure 5. Coarse Mesh: Pressure coefficient distribution for each turbulence model and Riemann Solver*

Globally, Figure 5 demonstrates quite a defined shape with not excessive variation among the different turbulence models. Additionally, both Riemann solvers - AUSM and ROE-FDS – present even less deviation, hence, we have decided to only graph RNG k-  $\varepsilon$  ROE as reference.

Then, we compute a further insight into figure 4 in the environment ( $x/c \sim 0.9$ ) where shape is the less homogenously sharped – let's say then, the most problematic point.

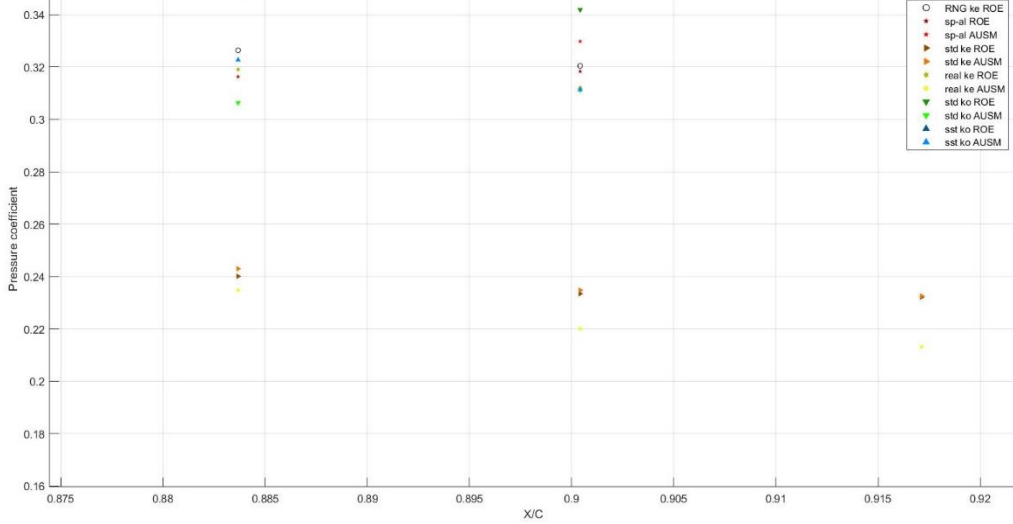


Figure 6. Insight into Figure 5

Figure 6 truly reveals the deviation from the turbulence models to the RNG  $k - \varepsilon$ . For  $x/c \sim 0.9$  the pressure coefficient is 0.32. The method which represents closest approach to our reference is Spalart-Allmaras with ROE-FDS solver, whose value is barely 0.32 as well. Additionally, we can find the furthest deviation in the Realizable  $k - \varepsilon$  model with AUSM solver, with a value of  $c_p \sim 0.21$ . This value represents a deviation of a 34.37% from the reference model. However, it must be considered that we are dealing with the worst scenario in the “worst” evaluated mesh too, so these values can take place.

We must also bear in mind that we are plotting deviations from the RNG  $k - \varepsilon$ , not from the experimental data, so the closest to the reference value does not imply more accurate solution. In fact, if we wanted to obtain it, we should compare these results with the values from Figure 2.

#### • Medium Mesh:

In this mesh, as declared in Table 1, the refinement factor of the defined surface for boundary layer has been 2. Hence, we should expect more “stability” and accuracy in the results

but also a significant increase in computational cost. Similarly to the Coarse Mesh, the residuals will be shown in Figure 7 and the total simulation time took 9:22.09 minutes, yet the convergence of solution has not been achieved either.

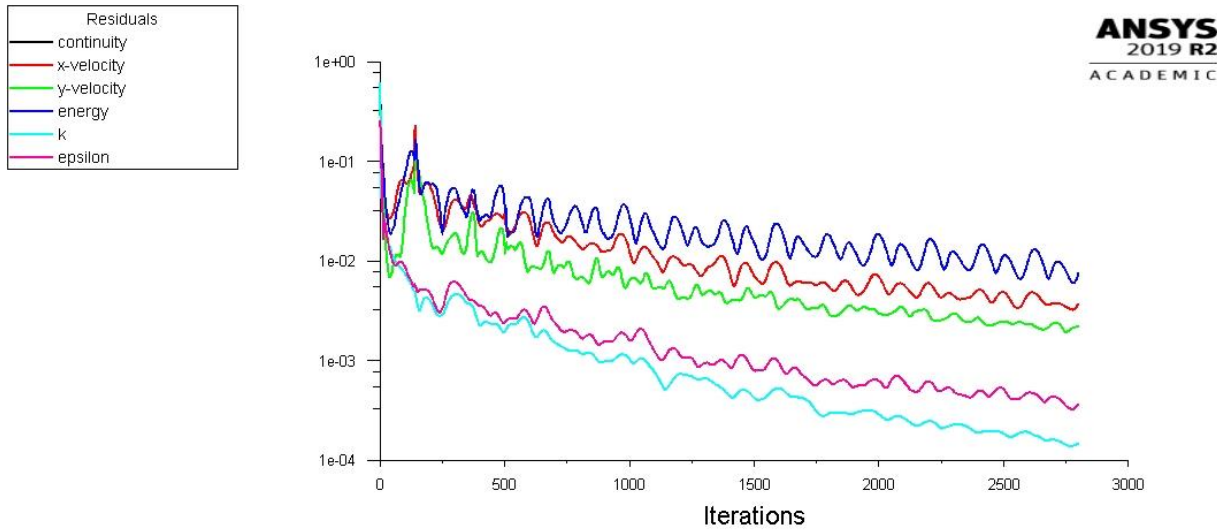


Figure 7. Scaled Residual for Medium Mesh, RNG  $k$ - $\varepsilon$  turbulence model

We will now perceive in Figure 8 that solution is definitely less scattered than it was on Figure 5 though.

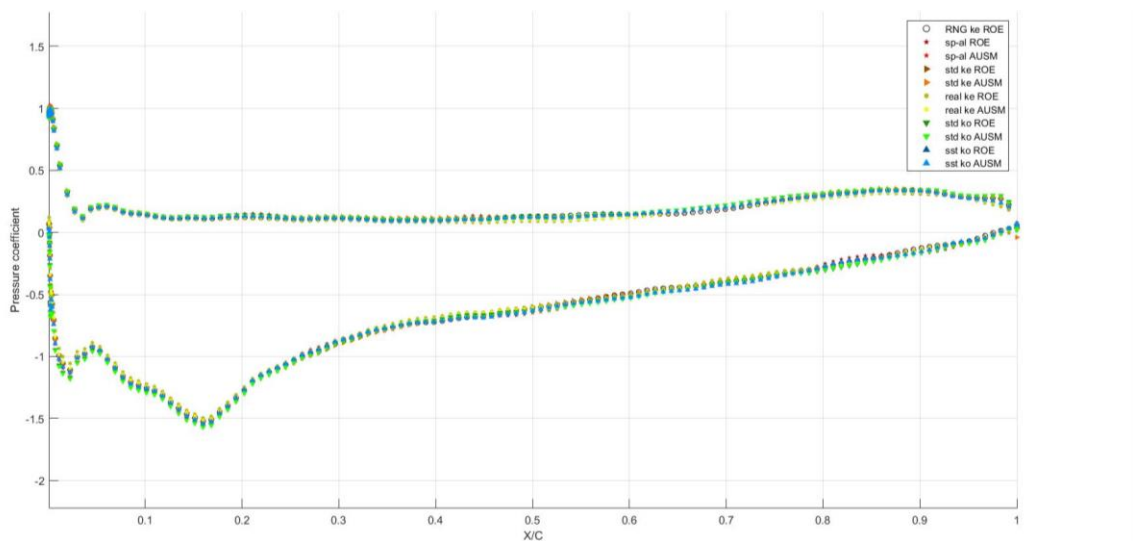


Figure 8. Medium Mesh: Pressure coefficient distribution for each turbulence model and Riemann Solver

As predicted, there is so little difference between the calculated pressure coefficient from each turbulence model but also between the two Riemann solvers as well.

By looking into our most problematic point ( $x/c \sim 0.9$ ), RNG  $k - \epsilon$  's  $c_p$  is 0.305. Actually, Realizable  $k - \epsilon$  is again the most deviated model with  $c_p$  is 0.275, and therefore varies 8,64% of the reference value. This consists a huge improvement in comparison with the data obtained in the Coarse Mesh in terms of accuracy to the solution.

#### • Fine Mesh:

At last, to configure our “Fine Mesh”, we have refined the boundary normal surface created with a refinement factor of 100. Due to this, an unstructured mesh will be created as we had in our Medium Mesh, aiming more accurate results without an excessive computational cost.

However, in this case we had the surprise of having converged results within 60 iterations in most of cases, which really was unexpected and rare. Intuition states that the longer the mesh, the further it should converge. From Coarse to medium, we struggled in obtaining “quasi-converged” results, hence we expected the same for this new case. This scenario can be seen in the residuals of Figure 9.

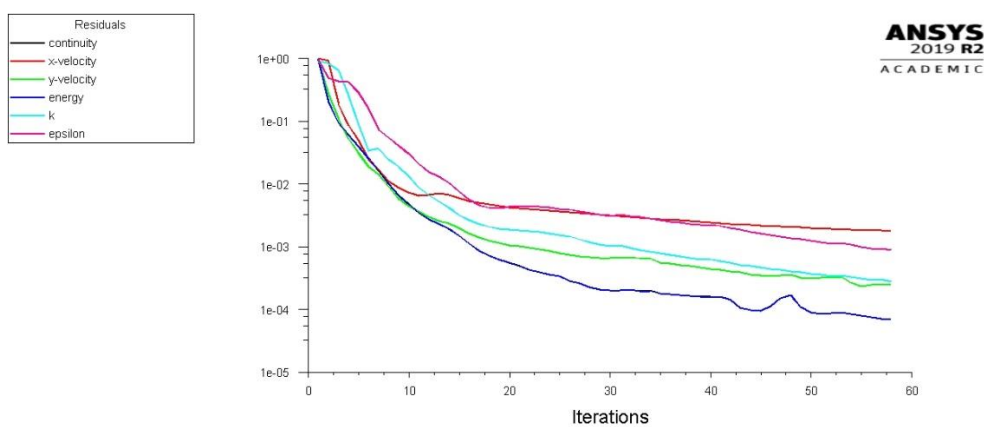


*Figure 9. Residuals for Fine Mesh and RNG  $k - \epsilon$  turbulence model, ROE-FDS solver. Converged solution at the 57<sup>th</sup> iteration*

Additionally, by looking into the results of Figure 10 it is displayed a clearly shaped and more detailed figure ( more points = more definition and information) than we had in our coarse mesh of Figure 5, nevertheless, it presents too little variation with the medium mesh. Moreover, practically there is so little difference between the different turbulence models as with the Riemann solvers as well.

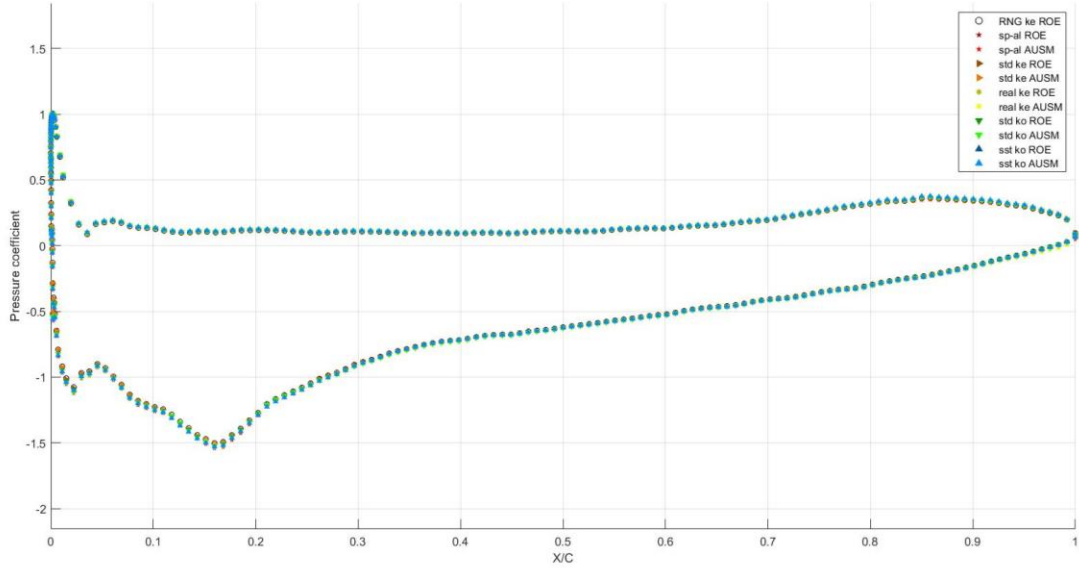


*Figure 10. Fine Mesh: Pressure coefficient distribution for each turbulence model and Riemann Solver*

If it was not the case that results converged so unexpectedly quickly for the fine mesh, it would be reasonable to compute the Medium mesh instead due to the minor computational cost. The insignificant difference of both results as can be seen in the following image.

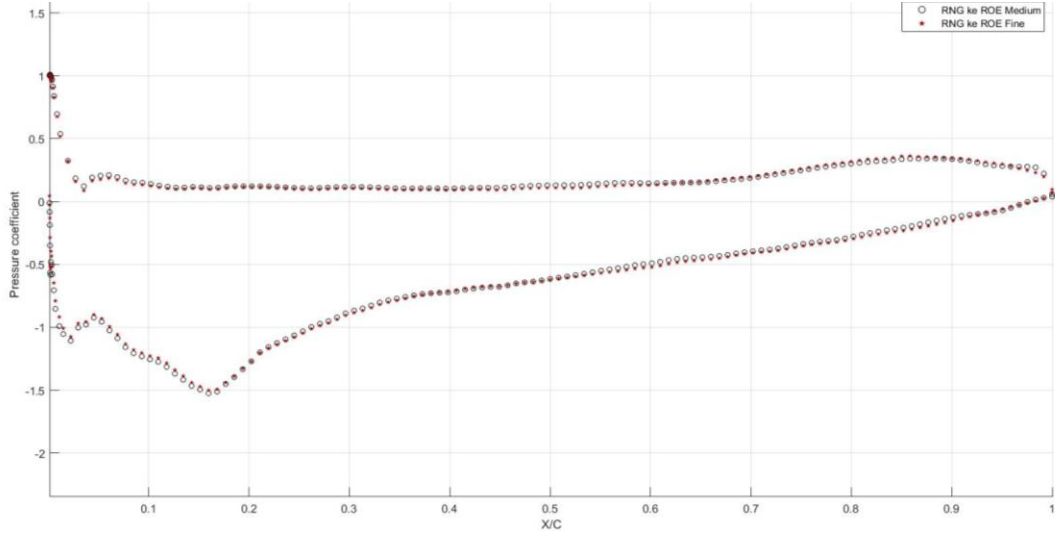


*Figure 11. Graphic Comparison between Medium and Fine Mesh*

## **Grid Convergence Study: Grid Convergence Index and Richardson Extrapolation.**

### **• Grid Convergence Index**

In order to ensure that our case ensures Validation and Verification criteria, a study of the Grid Convergence Index and Richardson Extrapolation will be carried out. The basis of the study method is withdrawn from NASA's webpage: (Roache, 1997)<https://www.grc.nasa.gov/WWW/wind/valid/tutorial/spatconv.html>, which is actually based on (Roache, 1997) the only validation and verification method for CFD available on literature.

Here, the results of the study will be presented and commented. See the further analysis and step-by-step procedure on Appendix 1.

For each mesh and using RNG  $k - \varepsilon$  turbulence model in conjunction with the Riemann ROE-FDS solver, we will evaluate the pressure coefficient value for the same x coordinate. As we

will show in the following images ( Figure 12, Figure 13, Figure 14 ) we have chosen a set of 7 strategic points which shallowly represent the shape of the pressure coefficient distribution. This proceeding will save considerable time to compute the GCI for all the points, but also represents neater conclusions and ensures that points will be common in the x coordinate for all the meshes.

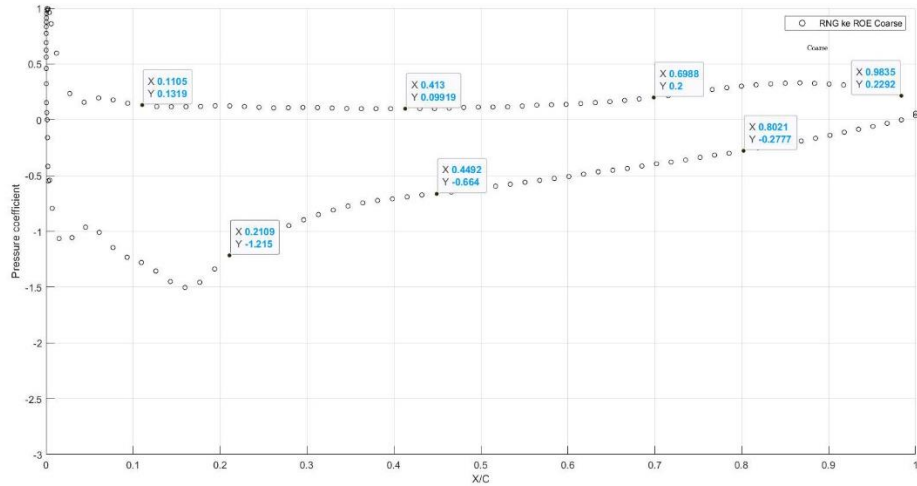


Figure 12. Points selection for COARSE Mesh

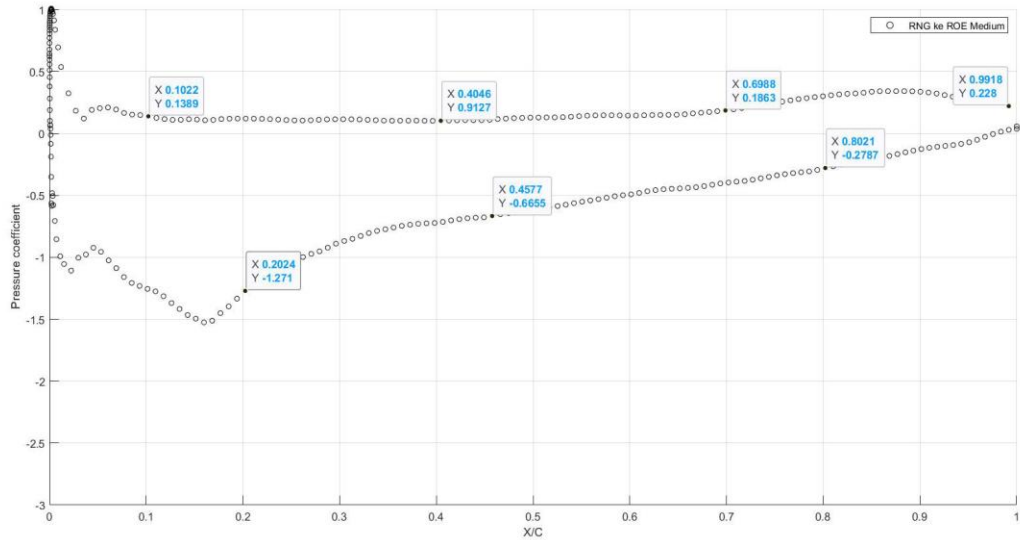
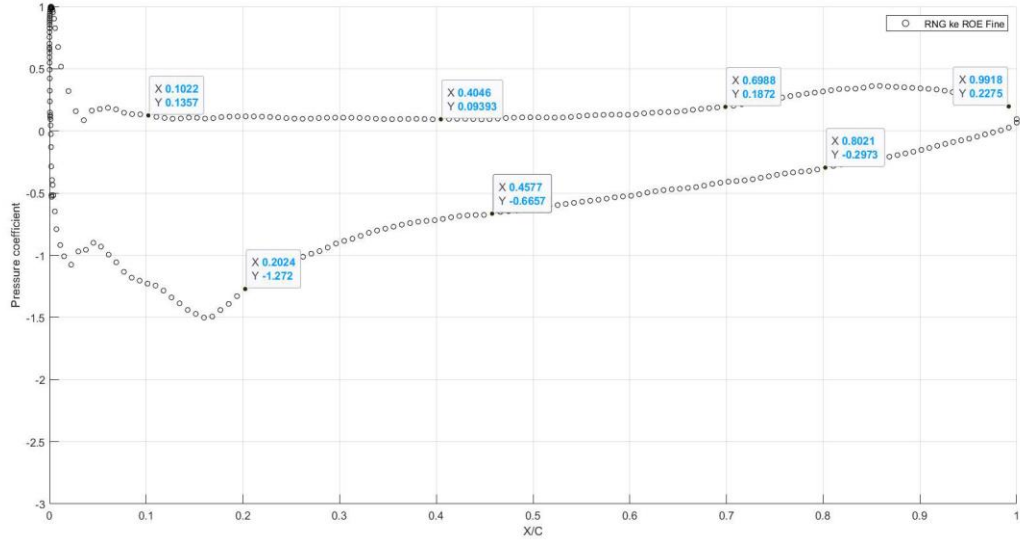


Figure 13. Points selection for MEDIUM Mesh



*Figure 14. Points selection for FINE Mesh*

Done this, we compute the grid convergence index 1-2 and 2-3 by analyzing the error convergence difference presented between meshes coarse-medium and medium-fine. Then, the indicated ratio will give us an idea about the real grid convergence index of the medium-fine mesh relatively to the coarse-medium. This ratio should follow an asymptote around the unitary value.

*Table 2. Grid Convergence Index*

x	Coarse	Medium	Fine	GCI 12	GCI 23	RATIO
0,1022	0,1319	0,1389	0,1357	2,410438	7,683699	2,303856
0,4046	0,09919	0,09127	0,09393	4,15047	9,227362	1,606797
0,6988	0,2	0,1863	0,1872	3,517287	1,566523	0,321892
0,9918	0,2292	0,228	0,2277	0,251737	0,357669	1,026872

---

0,8021	-0,2777	-0,2787	-0,2793	0,171618	0,699972	2,947801
0,40577	-0,6641	-0,665	-0,6657	0,064732	0,342626	3,825424
0,2024	-1,215	-1,271	-1,272	2,107379	0,256161	0,087852

---

These results may look like different from the theory of (Roache, 1997) but can be reasonable if we consider the following constraints:

- We have only refined the boundary-attached region and this fact makes that overall, the total number of cells does not grow excessively. Hence, ratios medium-coarse and fine-medium will not be greater than 2 (see Table 1) and this leads to a bigger GCI. For further information on the procedure, consider reading Appendix 1.
- A factor of safety of 1.25 has been applied, according to (Roache, 1997) when 3 meshes or more are evaluated, and these make GCI enlarge too.

Thus, and also keeping in mind the results graphed above (Figure 5, Figure 8, Figure 10), we can consider that errors converge as the mesh gets refined.

However, if it is noticed large results or a significant growth in the GCI, then it implies that mesh is over-refined and a coarsening factor should be therefore applied to guarantee GCI decreasing tendency.

### • Richardson Extrapolation

Using Richardson's extrapolation proposal, the "exact" solution will be computed by using the formula:

$$f_{exact} \approx f_2 + \frac{f_2 - f_1}{r^p - 1} \quad (4)$$

*Table 3. Richardson Extrapolation*

x	Coarse	Medium	Fine	RE 1-2	RE 2-3
0,1022	0,1319	0,1389	0,1357	0,14157848	0,12735858
0,4046	0,09919	0,09127	0,09393	0,08823949	0,10086381
0,6988	0,2	0,1863	0,1872	0,18105784	0,18954603
0,9918	0,2292	0,228	0,22775	0,22754083	0,22709833
0,8021	-0,2777	-0,2787	-0,2793	-0,27908264	-0,28086402
0,40577	-0,6641	-0,665	-0,6657	-0,66534438	-0,66752469
0,2024	-1,215	-1,271	-1,272	-1,29242783	-1,27460669

As it can be seen, extrapolated results for higher orders have been obtained by the extrapolation of the results from Medium-Coarse Mesh (RE 1-2) and for Fine-Medium Mesh (RE 2-3) in order to be able to compare the results from the Fine Mesh to the RE 1-2 , but also to

estimate a more accurate value with RE 2-3. Each extrapolation has been applied by considering,

$$r = \frac{\text{refined mesh number of cells}}{\text{coarser mesh number of cells}}$$
 and therefore  $r_{12} = 1.9009$ ,  $r_{23} = 1.1763$ . The order of convergence, p

is theoretically 2 as we have applied on the Grid Convergence Index.

## Conclusions

In this section, we will briefly discuss the most important outcomes of this document by commenting, in parts, the influence of the mesh, the turbulence models with different solvers, software used and the issues faced in the whole process.

The results from above state that finer meshes usually lead to more accurate and continuous solutions. However, as it can be seen, refinement is a double-edged sword which, if it has not been selected properly, might introduce undesirable effects in our solution. Additionally, it implies a significantly higher computational cost. Thus, the refinement of the mesh implies a compromise solution between the required accuracy and the computational cost you are disposed to arrange.

Another selection to be considered is the turbulence model applied. As it can be seen, specially for coarser meshes, it has a considerable impact in the solution, which may be even more noticed if turbulence is displayed in CFD post-processing. The most turbulence models used in the Aerospace Applications are Spalart-Allmaras due to its ability to withdraw quick solutions and SST  $k-\omega$  for its great performance in capturing turbulence in boundary section but also in the mean flow. However, our reference model has been RNG  $k-\varepsilon$  with 1<sup>st</sup> and 2<sup>nd</sup> order of convective flows, then all the other turbulence models analyzed have been commented referring to this one.

Although the Riemann Solvers conducted (ROE-FDS and AUSM) for the RANS equation base their performance on different mathematical models (see · Riemann Solvers.), it is found that solutions do not have significative deviations. Hence, for this case, the election of the Riemann Solver does not have great influence in the solution obtained.

The software used to run the simulations and to perform the whole process is Ansys Fluent, widely used in the Aerospace Industry. Although it is complete and user-friendly, it does not compute high-order schemes, which may be a huge constraint if high accuracy solutions are required. Furthermore, we have gained confidence and expertise in using this powerful tool, which was one of the main objectives of this module.

However, a lot of problems have been experienced until reaching the final results presented along this document. Most of the simulations have led to oscillatory or unacceptable solutions, hence the time to achieve reasonable outcomes has been excessive. It may be a good learning of the process of what real research and industry operations look like.

One issue that we have not been able to solve is the fact that convergence in the fine mesh is achieved within 60 iterations while for coarser mesh it takes much time. With my current little knowledge in simulations, I have not been able to describe the reason of this behavior. Thus, I look forward to gaining further experience in this topic.

I am also aware of the fact that I have exceeded the word limit. I should work harder on it in further assignments. Nevertheless, I tried to sum up this document but I was not happy with the result.

## **Future work**

The study case given provides further interesting steps to be completed. One of them, which has been proposed, is to analyze in depth the influence of the ground effect on this Tyrrell wing (see (David and Zerihan, 2001) and (Mahon and Zhang, 2005)). However, as commented previously, a lot of time has been spent in obtaining reasonable results from simulations due to a variety of issues occurring. Since more assignments need to be submitted, this interesting and even closer to reality step is held over to a near future where I have more available time. By the moment, a little introduction to this effect has been done in Appendix 2: Ground Effect Analysis.

Then, it would be also intriguing to compute more meshes with stable results in order to analyze with more basis the effects of the grid on the solution. Even it would be also interesting to generate the mesh or to look for other geometries, but in this module we did not have an introduction to grid generation due to limited time and efficiency; since our interest is mainly based in the analysis of the solution since mesh was decent for academic purposes.

## **Appendix 1: Grid Convergence Study.**

As seen in · Grid Convergence Index, the calculus of the grid convergence has been done under the procedure stated by NASA and (Roache, 1997)

In order to compute them and to have a reusable tool, we will use Microsoft Excel.

The first step to perform is to acquire several points from each mesh (with the same x-coordinate) that describe the solution curve. In our case, we determined the ones explained in the previous pages (see Figure 12, Figure 13, Figure 14).

Then, their difference in absolute value needs to be achieved and scaled by the minor value. The expression of this operation is the following:

$$\varepsilon_{21} = \frac{|f_2 - f_1|}{f_1}, \quad \varepsilon_{32} = \frac{|f_3 - f_2|}{f_2},$$

being  $f_1$ ,  $f_2$  and  $f_3$  the values of coarse, medium and fine mesh respectively. The order of the convergence of the solution is theoretical and depends on the numerical scheme applied. In our case the theoretical order of convergence is 2, nevertheless, in practice it can be calculated through:

$$p = \ln\left(\frac{|f_3 - f_2|}{|f_2 - f_1|}\right) / \ln(r)$$

Where the  $r$  value is known to be the ratio of refinement. Although in this document we have not refined the whole mesh (only a proximity-area of the boundary surface), it can express the ratio of cells of a finer mesh against a coarser mesh. For three meshes, we will logically have  $r_{21}$ ,  $r_{32}$  and  $r_{31}$  but only the two first will be considered in the process.

According to Roache, the Grid Convergence Index between two meshes relies on the formula:  $GCI = \frac{F_s \cdot |\varepsilon|}{r^p - 1} \cdot 100\%$

The only remaining factor to specify is  $F_s$ . According to Roache, it is desirable to have a safety factor whose value should be 3.0 if two meshes are compared or 1.25 for 3 three or more.

Overall, the GCI explains in terms of percentage the relative error bound; somehow, indicates the deviation from the finer mesh to the asymptote gathering the ideal solution. Thus, the smaller the GCI value obtained; the better performance will be achieved.

In the other hand, the GCI tends to be displayed in conjunction with the Richardson extrapolation. This method can acquire higher order of accuracy solutions through the extrapolation of discrete and less accurate values of the same function. The whole mathematical procedure can be seen in: (Anon, n.d.) but we will keep the final expression:

$$f_{h=0} = f_1 + \frac{|f_2 - f_1|}{r^p - 1}$$

As it has been already commented, the whole procedure has been accomplished in the Microsoft Excel software and the results can be seen in the following image:

MESHES VALUES				Errors			P	RE 2-3	RE 1-2	CGI 12	CGI 23	RATIO
x	Coarse	Medium	Fine	E12	E23							
0,1022	0,1319	0,1389	0,1357	0,050395968	0,02358143		2	0,127358576	0,141578478	2,410438	7,683699	2,303856
0,4046	0,09919	0,09127	0,09393	0,086775501	0,028318961			0,100863809	0,088239493	4,15047	9,227362	1,606797
0,6988	0,2	0,1863	0,1872	0,073537305	0,004807692			0,189546025	0,181057835	3,517287	1,566523	0,321892
0,9918	0,2292	0,228	0,22775	0,005263158	0,001097695			0,227098326	0,227540832	0,251737	0,357669	1,026872
0,8021	-0,2777	-0,2787	-0,2793	0,003588088	0,002148228			-0,280864017	-0,27908264	0,171618	0,699972	2,947801
0,40577	-0,6641	-0,665	-0,6657	0,001353383	0,001051525			-0,667524686	-0,665344376	0,064732	0,342626	3,825424
0,2024	-1,215	-1,271	-1,272	0,044059795	0,000786164			-1,274606695	-1,292427826	2,107379	0,256161	0,087852
Safety Factor				Ratios								
n=2	3			r12	r23							
n>=3	1,25			1,900900901	1,176276988							
Number of cells												
Coarse	Medium	Fine										
23976	45576	53610										

Figure 15. Grid Convergence Study using Microsoft Excel

## Appendix 2: Ground Effect Analysis

When studying CFD simulations of cars, the ground effect induced in the mean flow cannot be neglected at all. Hence, in this section, we will analyze and compare which perceivable consequences will be imposed by this boundary condition or phenomena.

The conditions of the free flow are the previous ones (see Characteristics of the Problem) except for the AoA (now it's  $3.6^\circ$  instead of  $5^\circ$ ) plus the contribution of the distance from the ground. This factor will be computed as the dimension-less new parameter of  $h/c$ , being  $h$  the height of the airfoil and  $c$  its cord.

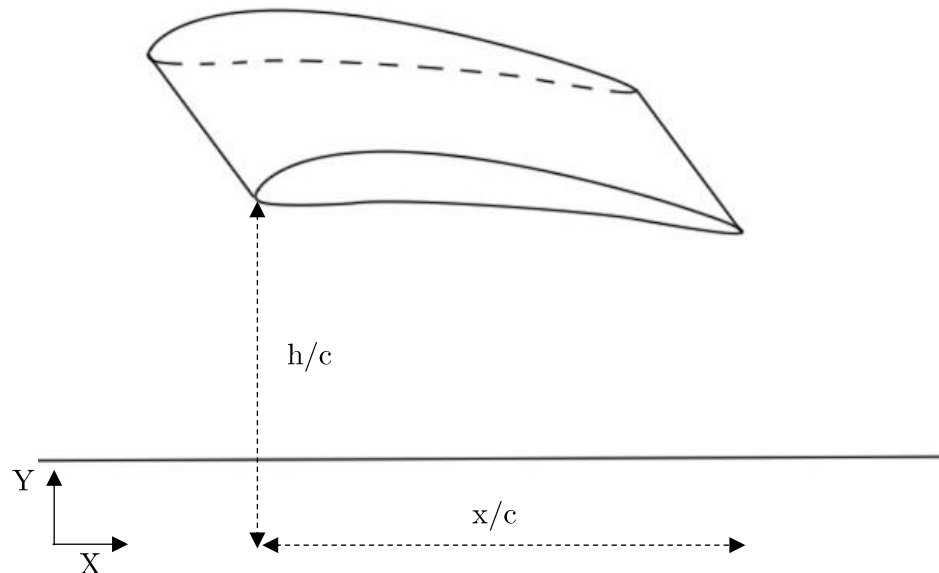


Figure 16. Scheme for the Airfoil-Ground effect with the dimensionless parameters

In the experimental study carried out by (David and Zerihan, 2001.) and (Mahon and Zhang, 2005), the value of  $h/c$  has been 0.224, therefore, we will use this value as well. Additionally, we have not refined the predetermined available mesh file “tyrrell\_3\_6\_degree\_hc\_0\_224\_ge”,

which contains exactly 42916 cells. As, by number of cells it approaches more to the medium mesh of the freestream case, we will compare it with this last case,

Overall, in a brief and qualitative insight (see (Jones and Smith, 2003)), the consequences of adding a ground effect to this airfoil lead to:

- For aviation with fixed-wings vehicles, the height from ground to the bottom surface of the wing is smaller, hence the pressure gradient, then vortical structures formed acquire elliptical-type shape instead of circular and there is a considerable reduction in induced aerodynamic drag.

Therefore, lift/drag coefficient is higher for the same environment conditions than for the freestream case, and consequently a certain amount of lift will be achieved with less AoA.

- In the contrary, for racing, the phenomena of ground effect are aimed in a distinct way. The idea is to create a high-pressure zone above the vehicle and low-pressure flow under the wing, then a downforce is originated instead of lift and grip (adherence) to the road is significantly boosted. Due to this, in curves, they can be more safely taken with higher speeds.

- It must be also considered the change of AoA from  $3.6^\circ$  (GE) to  $5^\circ$  in the case of freestream.

Once we take into account these considerations, we will plot the results for AoA  $3.6^\circ$  and  $5^\circ$  in ground effect against experimental data and computational RNG k- $\varepsilon$  turbulence model for AoA  $5^\circ$ .

An important issue faced in the problem is that the number of iterations of the ground effect mesh has been 3500 instead of the 1000 for the freestream case, since for 1000 the  $C_p$  did not look appropriately. This high number was chosen as a conservative factor, for further work it would be interesting to determine from which number of iterations results get reliable.

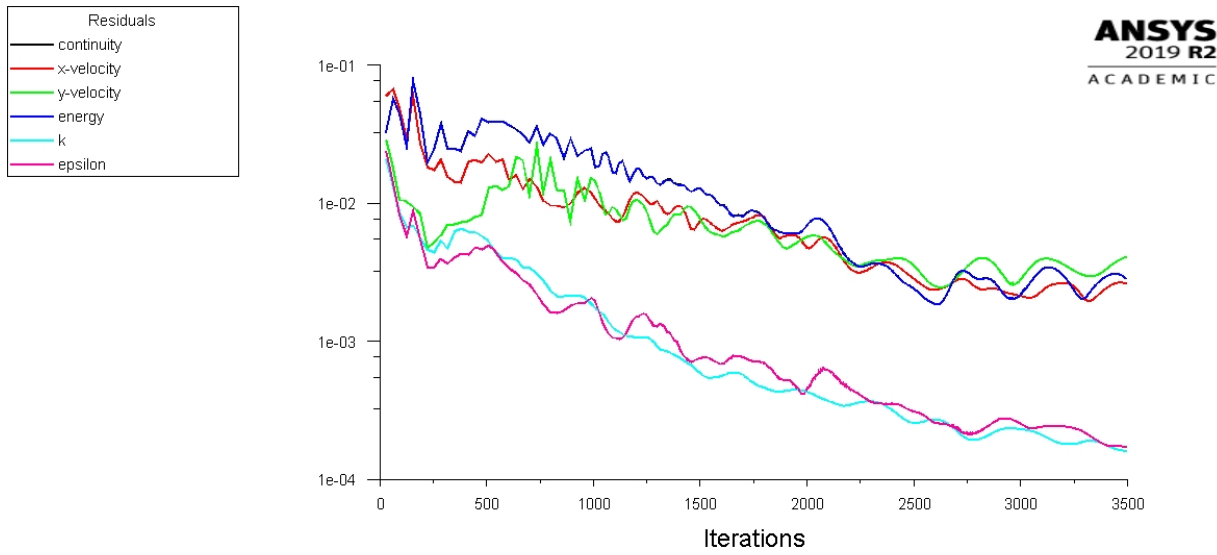


Figure 17. Residuals for Ground Effect Mesh

From Figure 17 residuals have not converged, nevertheless, they seem to start to oscillate

around a steady value. The results obtained are the following:

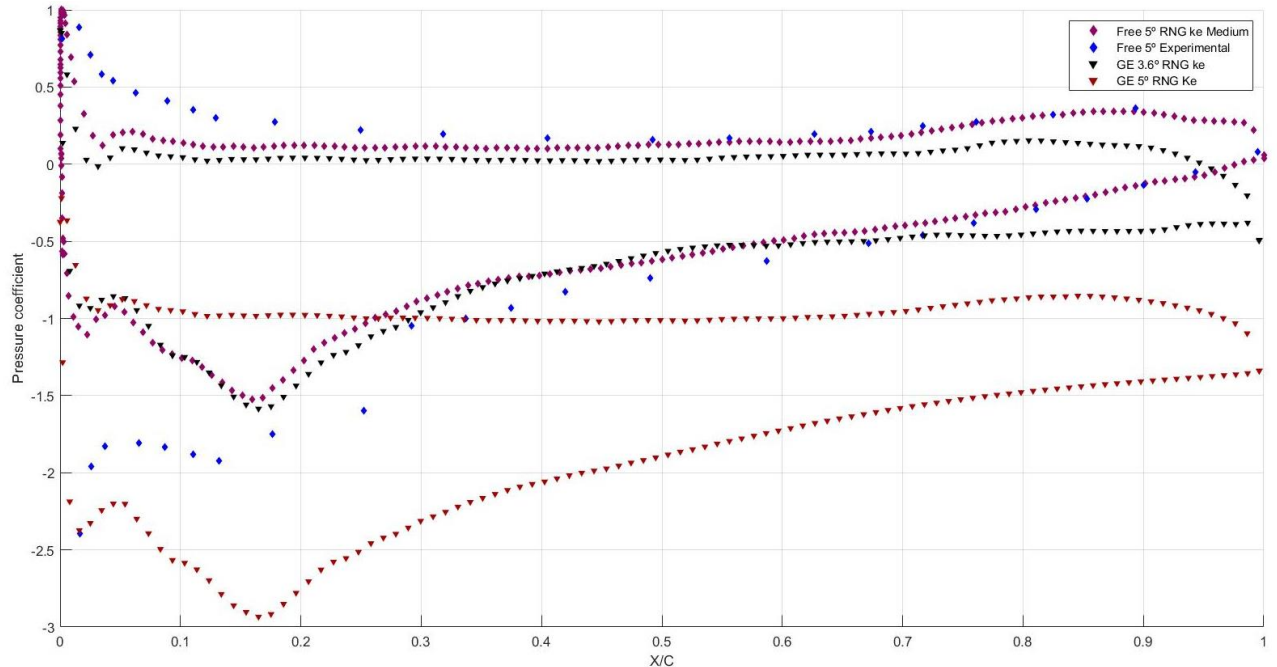
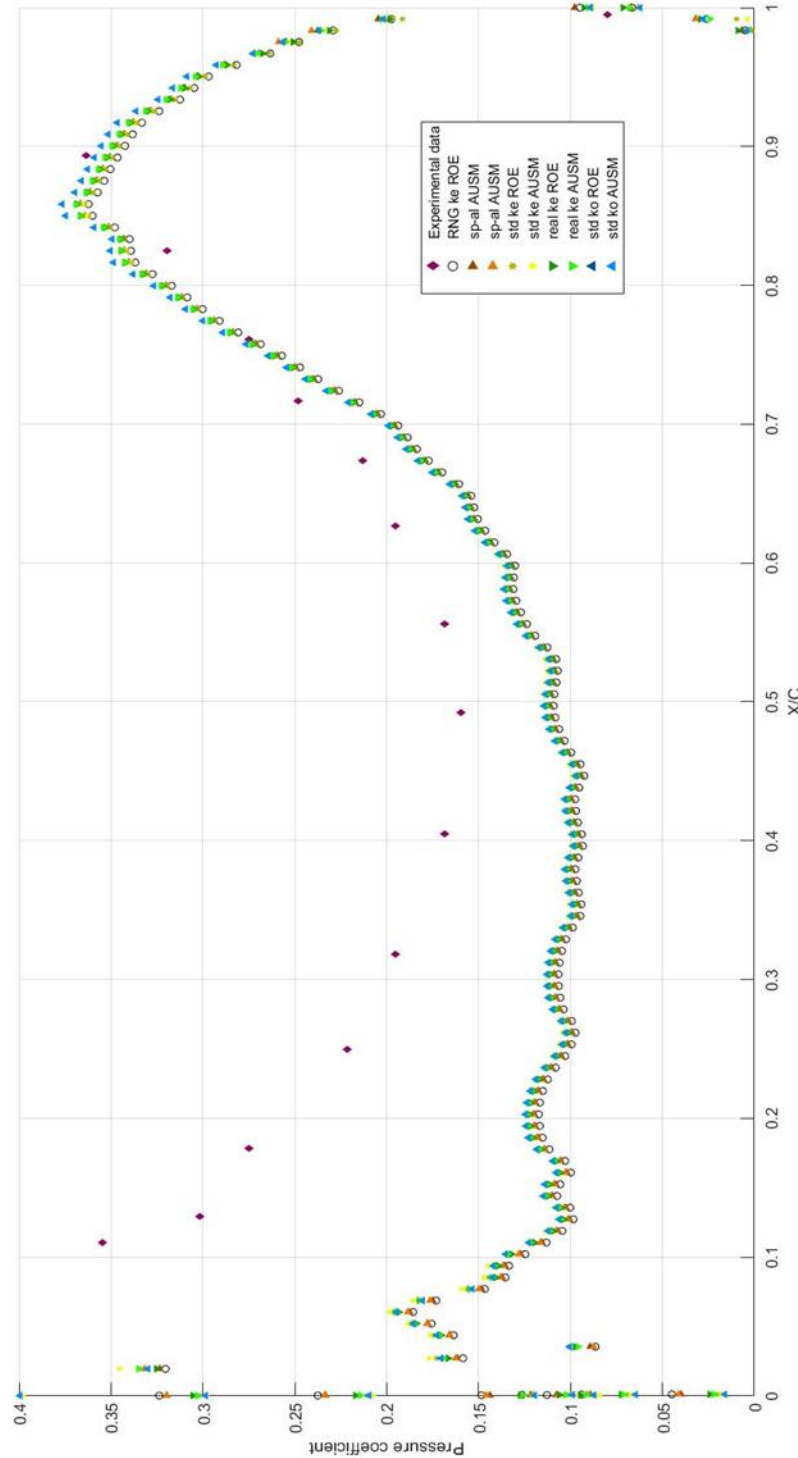


Figure 18. Ground effect of different Angle of Attack against Freestream Case

As it can be seen, in the trailing-edge region, the pressure coefficient for the 3.6° ground effect case gets lower values as expected. This effect can be highly boosted if the AoA is increased to 5°, where it gets negative values and subsequently the aimed ground-effect (downforce) is more significant. Since we are dealing with a Tyrrell racing car, this phenomenon is beneficial in terms of raising the safe speed and should be therefore looked for.

**Appendix 3. Large Image of Fine Mesh: Experimental data, Riemann Solvers, and turbulence models. Upper Airfoil Surface, Detail of Figure 10**



Upper region of the Tyrrell airfoil for Fine Mesh: Different Turbulence Models

## References

- NASA. *Examining Spatial (Grid) Convergence.* Available at:  
<https://www.grc.nasa.gov/WWW/wind/valid/tutorial/spatconv.html> (Accessed: November 27, 2019).
- David, J. and Zerihan, C. (2001.) *An Investigation into the Aerodynamics of Wings in Ground Effect.*
- Jakirlić, S., Eisfeld, B., Jester-zürker, R. and Kroll, N. (2007) “Near-wall, Reynolds-stress model calculations of transonic flow configurations relevant to aircraft aerodynamics,” *International Journal of Heat and Fluid Flow*, 28(4), pp. 602–615.
- Jones, M.A. and Smith, F.T. (2003) *Fluid motion for car undertrays in ground effect.*
- Mahon, S. and Zhang, X. (2005) “Computational analysis of pressure and wake characteristics of an aerofoil in ground effect,” *Journal of Fluids Engineering, Transactions of the ASME*, 127(2), pp. 290–298.
- Roache, P.J. (1997) *QUANTIFICATION OF UNCERTAINTY IN COMPUTATIONAL FLUID DYNAMICS.*